Supporting Information

Transient Absorption Imaging of P3HT:PCBM Photovoltaic Blend: Evidence For Interfacial Charge Transfer State

Giulia Grancini [a], *Dario Polli* [a,b], *Daniele Fazzi* [b], *Juan Cabanillas Gonzalez* [c], *Giulio Cerullo* [a], *Guglielmo Lanzani*[a,b]

[a]CNR-INFM Dipartimento di Fisica, Politecnico di Milano, Piazza L. da Vinci, 32, 20133 Milano, Italy,

[b]Center for NanoScience and Technology CNST-IIT@POLIMI, via Pascoli 70/3, 20133 Milano, Italy,

[c]Madrid Institute of Advanced Studies, IMDEA Nanociencia, Faculdad de Ciencias, Av. Tomas y Valiente 7, 28049 Madrid, Spain

E-mail: guglielmo.lanzani@iit.it

RECEIVED DATE

S1. Experimental Setup

The experimental setup of the ultrafast confocal microscope is shown in Figure S1. It is driven by 10-μJ, 150-fs pulses at 1kHz repetition rate and 800 nm wavelength produced by an amplified Ti:Sapphire laser (Quantronix model Integra-C). The fraction of the pulse energy reflected by a first beam splitter (BS1 in the figure S1) is frequency doubled passing through a second-harmonic crystal to generate the pump pulses at 400 nm. The transmitted part is focused in a sapphire plate to produce a single-filament

white light continuum spanning the 450-800 nm wavelength range, used as a probe. Pump and probe pulses, synchronized by a computer-controlled delay line with ~5-fs accuracy, are collinearly recombined by a dichroic beam splitter (BS2 in the figure) and focused on the sample by a high numerical aperture air microscope objective (100×, NA=0.75).

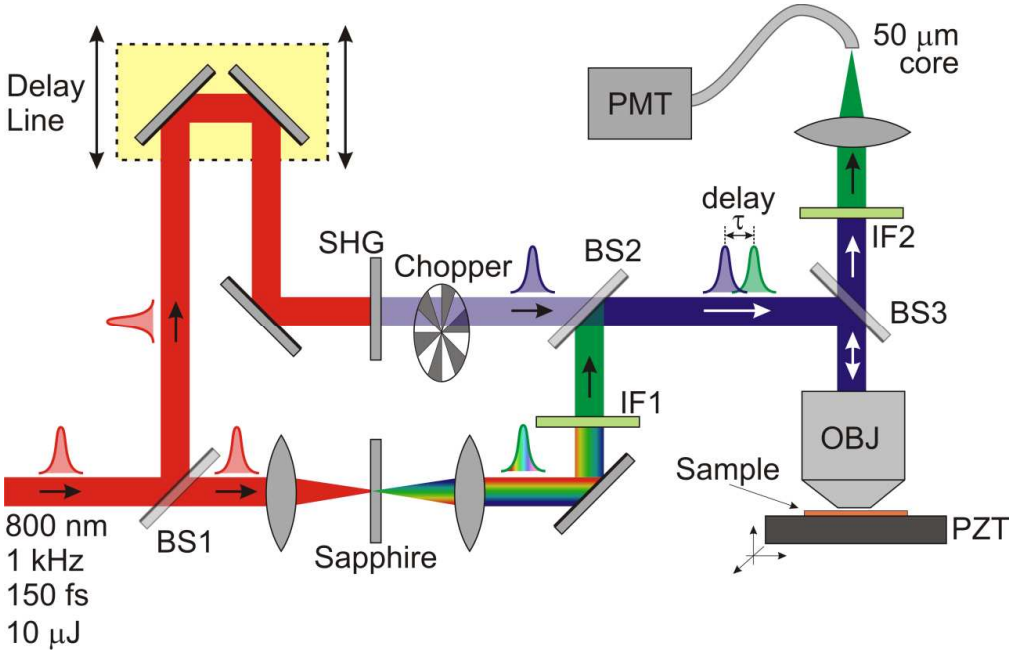

Figure S1: Experimental setup of the ultrafast confocal microscope. BS1 and BS3 are 50% beam splitters, while BS2 is a dichroic beam splitter. SHG: second harmonic generation crystal; OBJ: microscope objective; PZT: piezo-translator; PMT: photomultiplier; IF: interference filter.

The sample is raster scanned by a piezotranslator with nm accuracy on a 100x100 μm^2 scan area, thus allowing the acquisition of three-dimensional linear transmission $T(x,y,\lambda)$ images as a function of sample position (x,y) and probe wavelength λ. By modulating the pump beam with a mechanical chopper and demodulating the collected probe light at the same frequency, we also simultaneously register four-dimensional differential transmission $\Delta T/T(x,y,\lambda,\tau)$ images, which also depend on the pump-probe delay τ. We usually exploit our Four-Dimensional capability by first collecting a high-resolution two-dimensional $\Delta T/T$ (x,y) images at a few fixed pump-probe delays and probe wavelengths,

in order to highlight the morphological structure and to identify the (x,y) coordinates of the interesting features occurring in the sample; secondly, we move to these spots of the sample and we record pump-probe $\Delta T/T(\tau)$ dynamics at selected probe wavelength in order to precisely extract the associated kinetics and time constants. The minimum detectable signal is $\Delta T/T \sim 10^{-4}$.

Our instrumental temporal and spatial resolutions are 150 fs and 300-400 nm, depending on probe wavelength.

S2. Sample preparation

The solution of P3HT:PCBM (weight ratio 1:1) in dichlorobenzene (15mg/mL) was heated and stirred for one hour at 70° C. The solution was casted by slowly spin coating (800 rpm for 10 seconds) on a metal substrate leading to a sample with homogeneous thickness of few hundreds of nanometers. The preparation of the sample was performed in an inert gas atmosphere inside the glove box. The thermal annealing procedure, was accomplished by placing the film on a hot plate at 140° C for 12 minutes under nitrogen atmosphere. By thermal annealing we thermodynamically alter the phase separation of the blend ensuring high crystalline order and purity within each phases. We tailor the degree of phase separation so that PCBM-rich crystal domains and ordered P3HT- rich regions are built up. Therefore our sample is made of PCBM-rich clusters immersed in a mostly fibrillar-like P3HT crystals and amorphous P3HT region [1,2,3,4]. The samples were measured and in ambient conditions. The film thickness ensures that all possible metal induced effects are negligible.

S3. Confocal linear transmission map and pump probe image on a 10x10 μm^2 area

The linear confocal transmission map, (Figure S2a), shows an artificially coarsened phase separation between P3HT and PCBM.

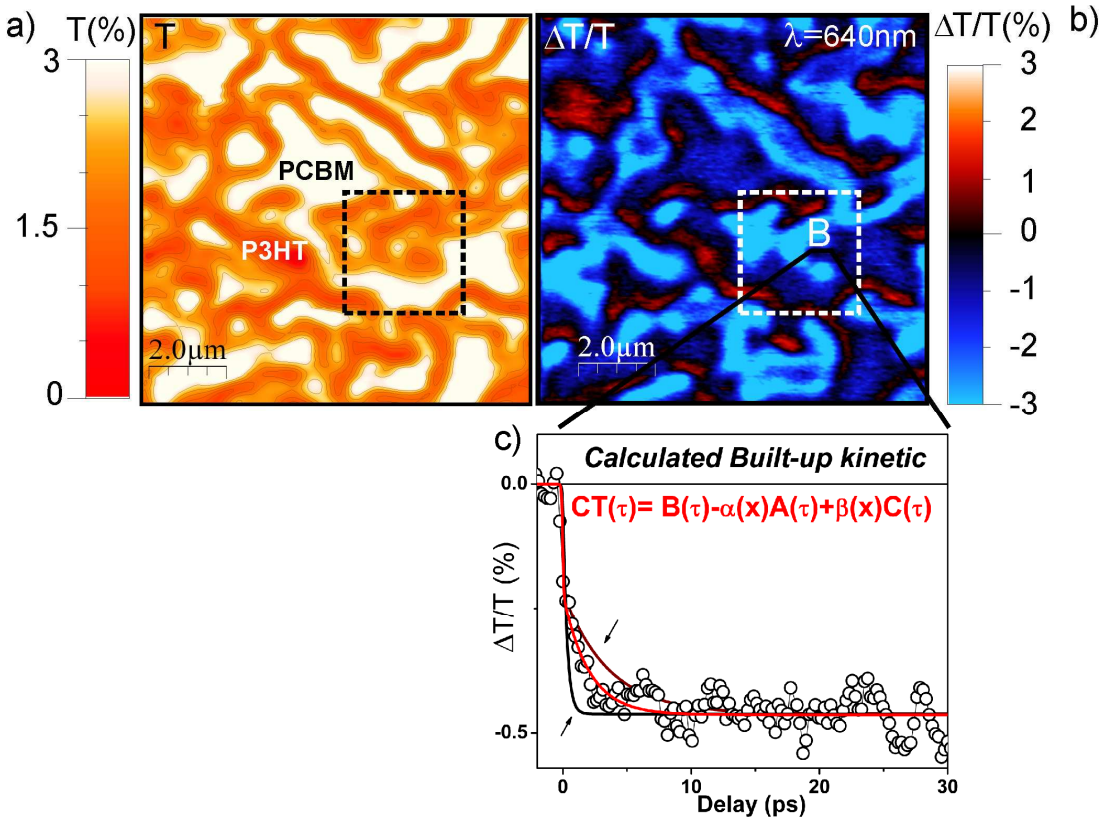

Figure S2: (a, b) Linear transmission and pump-probe confocal maps of P3HT:PCBM blend. a, Linear confocal transmission map. b, ΔT/T(x,y) map collected at τ=200fs pump-probe delay and λ=640 nm probe wavelength. Both the images are simultaneously collected in the same 10x10 μm^2 area at; scalebar: 2 μm. **(c)** Calculated Build-up CTS dynamic as $CT(\tau)=B(\tau)-\alpha A(\tau)+\beta \cdot C(\tau)$ at the interface; fits with confidence interval, depending on the choice of α and β. The coefficients α and β, which are adjust for fitting, are bound to follow a simple increasing (decreasing) trend in moving from A to C.

The blend is made of single PCBM-rich crystals, (appearing white in the optical image), coexisting with sub-micron elongated P3HT-rich domains, (in a darker orange color in the map). Note that both a crystalline phase of P3HT and an amorphous one could coexist in the blend. The presence of these two phases is hard to recognize just from the optical contrast image, as well as interfacial region between the crystallites. On the contrary the confocal map gives us much richer information, enabling us to investigate different photophysics and dynamical pathways related to the local environment. In particular Figure S2b shows the simultaneous pump probe ΔT/T(x,y) map collected at τ=200fs pump-

probe delay and λ=640 nm probe wavelength on a 10x10 μm^2 area. At this probe wavelength the image shows a spatially varying signal due to the presence of different pump-probe signal from amorphous P3HT/cristalline P3HT or PCBM -rich regions.

The marked dashed area represents the zoomed region discussed in the paper. As discussed in the paper the peculiar CT feature comes from the border region between P3HT and PCBM rich-crystallites. Here we show the extracted dynamic, presented and commented in detail in Figure 2d of the paper, together with the fitted curves. The dynamic represent the formation of the peculiar CTS at the border region and it is described by $CT(\tau)=B(\tau)-\alpha(x)\cdot A(\tau)+\beta(x)\cdot C(\tau)$. In particular, even if some arbitrariness in the choice of α and β is introduced, yet, because both A(t) and C(t) decay to about 10-20% of the initial value, while B(t) is constant with time, this uncertainty is not relevant. The main uncertainty is in the build-up kinetics up to 30 ps, as shown by the confidence interval by brown and black curves in Figure S2c.

In order to elucidate the signal detected by the confocal map we measured the pump probe dynamics on separate pristine films made of pure phases, looking in particular at 640nm probe wavelength, particularly interesting for our discussion.

S4. Pump probe spectra

Standard pump-probe spectra on both pristine materials and the blend under investigation, as measured on ~150 μm spot, are measured and used as references for interpretation of the confocal signal. Figure S3 shows the spectral evolution of the pump-probe signal from 200fs to 100ps time delay. In the pristine cristalline-P3HT film (Figure S3 Panel I) [5, 6, 8] it is possible to distinguish three ground state photobleach (PB) contributions, which produce a positive signal. These correspond to 0-0,0-1,0-2 (increasing energy) absorption transition, where the pronounced vibronic feature at 600nm is due to high crystallization order. At around 620nm a photobleaching (PB) signal overlaps with Stimulated Emission (SE). The ΔT/T signal turns negative above 630 nm due to overlap with photoinduced absorption (PA), but SE extends to at least 650 nm, as visible in longer time traces (Figure S3, Panel I, blue line). The PA

band that peaks at 640 nm is assigned to interchain charge-pairs that are instantaneously photogenerated in the pure crystalline P3HT phase [6,8].

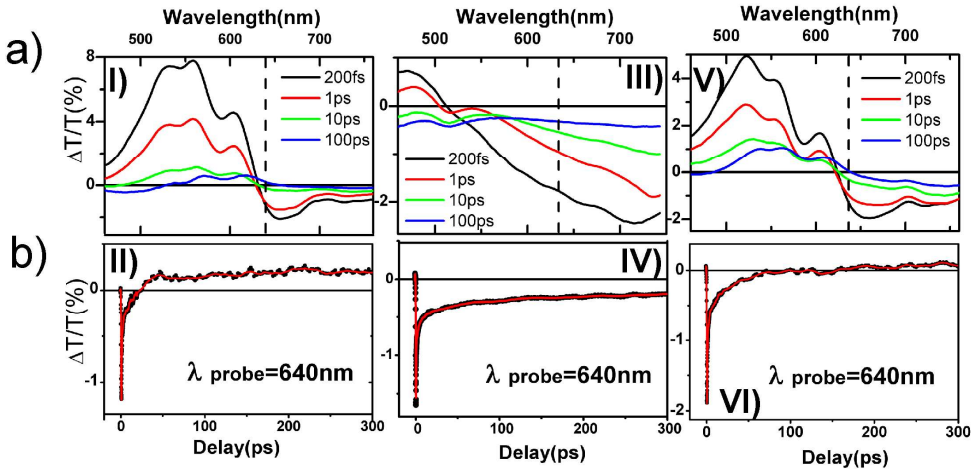

Figure S3: (a) Pump-probe spectra averaged on 150 μm diameter spot and (b) temporal decay of PA signal at λ=640nm in: Panel I, II, rr-P3HT pristine; Panel III, IV pristine PCBM; Panel V, VI P3HT:PCBM (1:1) finely dispersed blend upon thermal annealing. Different colors represent the temporal spectral evolution up to 100 ps. Pump beam is at λ=400nm wavelength at 150nJ/cm^2 excitation intensity.

In Figure S3 Panel III the pure PCBM pump probe spectrum is shown. Here we could identify PB at shorter wavelength (up to 500nm) and a broad PA band due to singlet-singlet absorption at longer ones [6,7]. Note that the charge band is out of our spectral window, peaking around 1050nm. [7]

Upon blending P3HT with PCBM a new decay channel for the neutral states becomes available, due to charge separation at the interface. This results in the conversion of P3HT singlets into positive polarons. In the standard pump probe spectrum, shown in Figure S3 Panel V, the PA feature at [630-700] nm appears much stronger and longer-lived compared to the pristine polymer. This band has now contributions from Coulombically bounded P3HT$^+$/PCBM$^-$ Charge Transfer State (CTS), quenching the SE signal. Note that the absorption spectrum of the CTS is similar to that of charge-pairs in pure P3HT,

probably because of the similar Coulomb interaction and inter-charge separation in the two states. Note that the signal decays almost to zero after 100ps, thus indicating geminate recombination of this CTS in this finely dispersed morphology. From these experiments we get a very important notion: *the PA band in the 630-700 nm spectral range is a finger print of the CT state.* For this reason we tune our probe to 640nm wavelength, in order to spatially imaging the CTS signal. Note that Similar features have also been observed by probing the CTS dynamics in the near IR region at 740nm wavelength.

S5. Depolarization Map

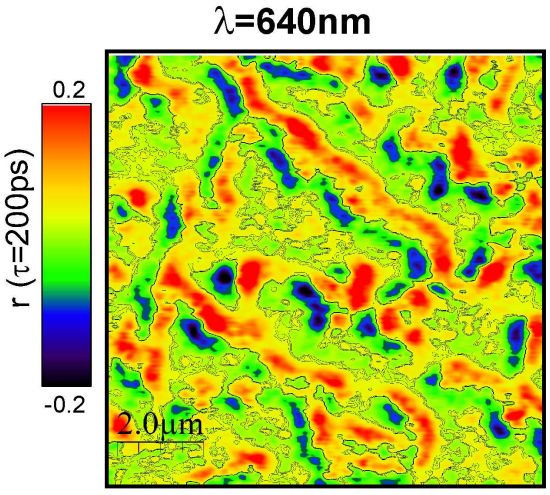

Figure S4: De-polarization Memory images of the P3HT:PCBM blend and temporal traces of the anisotropy decay r(τ). a) 10x10 μm^2 r(x,y) image at λ=640 nm probe wavelength and τ=200 ps pump-probe delay; scalebar: 2μm.

Figure S4 displays the *depolarization map*, reporting the values of *r* (as calculated from Eq 2) collected at λ=640 nm probe wavelength and τ=200 ps delay. Remarkably, we find a spatial distribution of *r*, with regions displaying different absolute values and signs. In particular the negative regions (blue in the image) are related to border region between P3HT and PCBM –rich phases.

S6. Theoretical calculations

Molecules theoretically investigated in this report are PCBM and P3HT polymer. To describe, from a computational point of view, the P3HT polymer we considered a representative finite size oligomer with six thiophene rings; the oligomer length herein considered well reproduce the electronic and optical properties of the whole polymer [9] and, moreover, it is longer than the average PCBM size. In this way P3HT oligomer fully contains the whole projection of PCBM structure.

Single molecular structures of PCBM and P3HT oligomer, have been optimized by using the semiempirical Hartree-Fock method AM1 [10]; also DFT optimized geometries (i.e. B3LYP/3-21G* [11]) have been obtained with no significant differences on the overall structures.

P3HT:PCBM interface has been modeled starting from single optimized molecular structures and superimposing them in order to obtain a supramolecule (named dimer). The intermolecular distance between PCBM and P3HT in the dimer has been set around 3.4-3.5 Å, as reported in literature studies [9, 11, 12].

Three different relative orientations (see Figure S5) between PCBM and P3HT molecules have been considered for the dimer structure, such as: 1) a pentagon of PCBM faced to a thiophene ring of P3HT, 2) a hexagon of PCBM faced to a thiophene ring and 3) two hexagonal faces of PCBM faced to P3HT. For each of these three relative orientations (1-3) we investigated the influence of the inter-molecular distance on the low excited states properties (e.g. transition dipole moments, polarization and energies) by considering also other inter-molecular distances than 3.5 Å, such as: 4.5 Å and 5.5 Å.

For each case (i.e. 1-3) and for each distance, the dimer structures have been kept frozen and not re-optimized [13-17]. We are conscious that the choice of avoiding any geometrical relaxation, both in terms of intra-molecular structural reorganization and inter-molecular readjustments, strongly affects the optical properties of the heterostructure (P3HT:PCBM); for this reason we build our dimer structures referring to consolidate theoretical and experimental results [9, 12-14] verifying that our data (i.e. molecular orbitals) are consistent with the literature ones [9, 12].

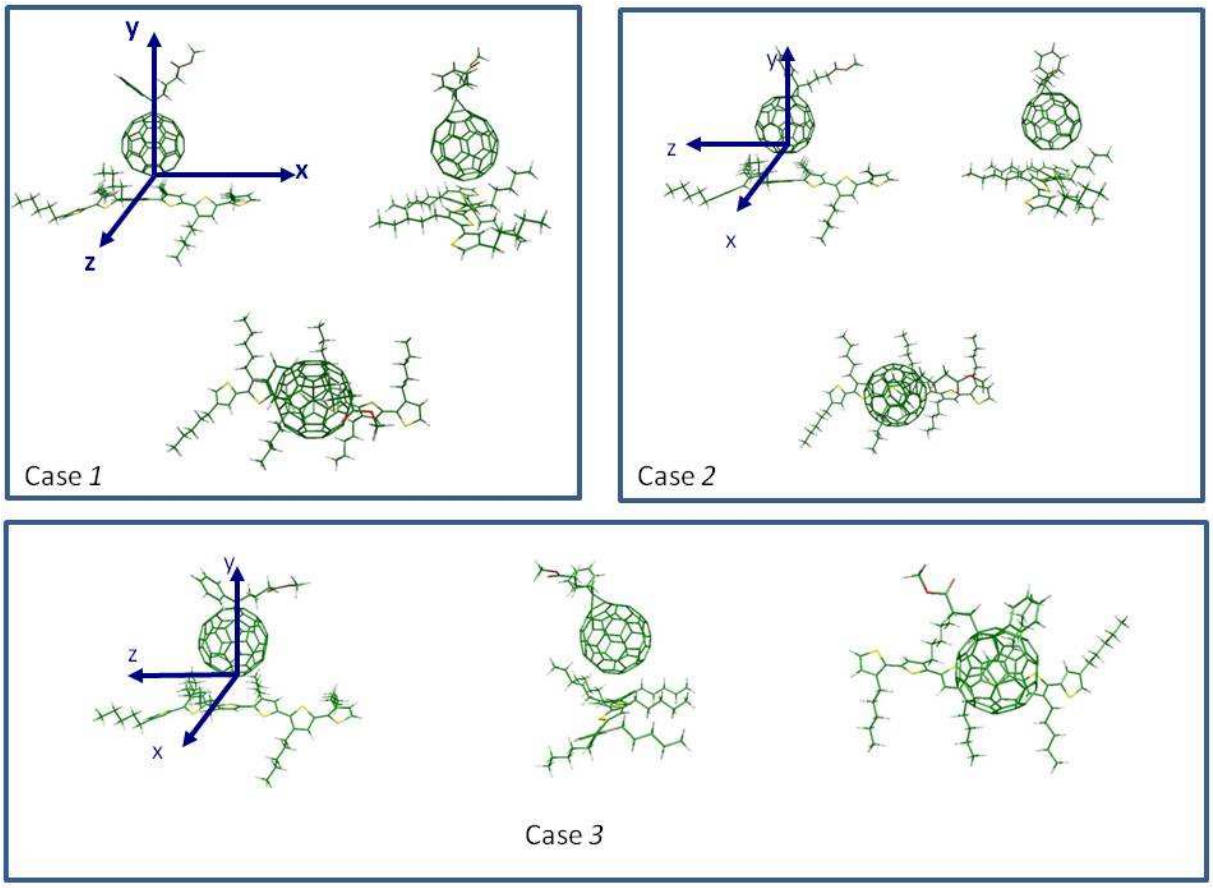

Figure S5: Three cases (1-3) different relative orientations between PCBM and P3HT molecules considered in this study. Geometries of the single molecules have been previously optimized by using AM1 method.

To characterize the excited states properties of each dimer we adopted both a semiempirical ZINDO/S method [18], widely used for organic systems especially combined with the AM1 method [16, 17] and, upon the optimized DFT structures, the TD-DFT method adopting TD-CAMB3LYP/3-21G* level of theory. The use of Coulomb Attenuated Method has been used in order to avoid the well known problem of the low lying intruder states as documented for the B3LYP functional [19]. In order to study the effect of the basis set also TD-CAMB3LYP/6-31G** calculations have been carried out on the supramolecular complex, but no significant variations respect to the 3-21G* case have been found (see Panel S6 and

S7). Due to the huge amount of atoms to treat at the ab-initio level, TD-DFT calculations have been carried out only for the first 30 excited states of the molecular complex (i.e. P3HT:PCBM), see Panel S6 and S7. For each supramolecular configuration (cases 1-3) we calculated instead more than 100 excited states at the ZINDO/S level. To study the effects induced by electronic and excitonic interactions, the dimer excited states properties have been compared with those calculated for the single isolated molecules. By varying the inter-molecular distance between PCBM and P3HT (i.e. 4.5 Å and 5.5 Å), we observed that the lowest excited states of the P3HT:PCBM complex tend to coincide with those of the isolated non interacting molecules.

Excited State	1:	2.6226 eV	472.76 nm	f= 0.0015
Excited State	2:	2.6349 eV	470.55 nm	f= 0.0015
Excited State	3:	2.6679 eV	464.73 nm	f= 0.0003
Excited State	4:	2.6783 eV	462.92 nm	f= 0.0004
Excited State	5:	2.7538 eV	450.23 nm	f= 0.0001
Excited State	6:	2.7650 eV	448.40 nm	f= 0.0000
Excited State	7:	2.8201 eV	439.64 nm	f= 0.0014
Excited State	8:	2.8991 eV	427.66 nm	f= 0.0001
Excited State	9:	2.9310 eV	423.01 nm	f= 0.0000
Excited State	10:	3.0155 eV	411.15 nm	f= 0.0000
Excited State	11:	3.0305 eV	409.12 nm	f= 0.0004
Excited State	12:	3.0451 eV	407.16 nm	f= 0.0001
Excited State	13:	3.1864 eV	389.11 nm	f= 0.0023
Excited State	14:	3.2199 eV	385.06 nm	f= 0.0023
Excited State	15:	3.2509 eV	381.39 nm	f= 0.0008
Excited State	16:	3.2571 eV	380.66 nm	f= 0.0006
Excited State	17:	3.3443 eV	370.73 nm	f= 0.2883
Excited State	18:	3.3691 eV	368.00 nm	f= 0.9596
Excited State	19:	3.4080 eV	363.81 nm	f= 0.2346
Excited State	20:	3.4380 eV	360.63 nm	f= 0.0155
Excited State	21:	3.4735 eV	356.94 nm	f= 0.0053
Excited State	22:	3.5733 eV	346.98 nm	f= 0.0055
Excited State	23:	3.5920 eV	345.17 nm	f= 0.0001
Excited State	24:	3.6520 eV	339.49 nm	f= 0.0022
Excited State	25:	3.6895 eV	336.05 nm	f= 0.0117
Excited State	26:	3.8670 eV	320.62 nm	f= 0.0148
Excited State	27:	3.8772 eV	319.78 nm	f= 0.0053
Excited State	28:	3.8923 eV	318.54 nm	f= 0.0019
Excited State	29:	3.9272 eV	315.71 nm	f= 0.0157
Excited State	30:	3.9337 eV	315.19 nm	f= 0.0028

Panel S6: TD-CAMB3LYP/3-21G* excited state energies of the P3HT:PCBM complex.

Excited State	1:	2.5066 eV	494.64 nm	f= 0.0013
Excited State	2:	2.5366 eV	488.78 nm	f= 0.0000
Excited State	3:	2.6079 eV	475.42 nm	f= 0.0000
Excited State	4:	2.6270 eV	471.96 nm	f= 0.0000
Excited State	5:	2.7548 eV	450.07 nm	f= 0.0002

Excited State	6:	2.7870 eV	444.87 nm	f= 0.0001
Excited State	7:	2.8017 eV	442.53 nm	f= 0.0008
Excited State	8:	2.8611 eV	433.34 nm	f= 0.0000
Excited State	9:	2.8835 eV	429.98 nm	f= 0.0001
Excited State	10:	2.8994 eV	427.63 nm	f= 0.0008
Excited State	11:	2.9336 eV	422.64 nm	f= 0.0010
Excited State	12:	3.0067 eV	412.36 nm	f= 0.0091
Excited State	13:	3.0528 eV	406.13 nm	f= 0.0028
Excited State	14:	3.0794 eV	402.63 nm	f= 0.0013
Excited State	15:	3.0995 eV	400.01 nm	f= 0.0006
Excited State	16:	3.1273 eV	396.46 nm	f= 0.0008
Excited State	17:	3.2172 eV	385.38 nm	f= 0.2745
Excited State	18:	3.2392 eV	382.76 nm	f= 0.1784
Excited State	19:	3.2626 eV	380.02 nm	f= 1.0004
Excited State	20:	3.4796 eV	356.31 nm	f= 0.0050
Excited State	21:	3.5039 eV	353.85 nm	f= 0.0003
Excited State	22:	3.5820 eV	346.13 nm	f= 0.0070
Excited State	23:	3.6265 eV	341.88 nm	f= 0.0004
Excited State	24:	3.6675 eV	338.06 nm	f= 0.0045
Excited State	25:	3.7569 eV	330.01 nm	f= 0.0064
Excited State	26:	3.7655 eV	329.26 nm	f= 0.0082
Excited State	27:	3.7766 eV	328.29 nm	f= 0.0031
Excited State	28:	3.8108 eV	325.35 nm	f= 0.0126
Excited State	29:	3.8274 eV	323.94 nm	f= 0.0010
Excited State	30:	3.8401 eV	322.87 nm	f= 0.0015

Panel S7: TD-CAMB3LYP/6-31G** excited state energies of the P3HT:PCBM complex.

In Figure S8 we report the excited states vertical transitions (ZINDO/S) for the dimer of case 1 by considering different intermolecular distances namely 3.5, 4.5 and 5.5 Å. For the other relative orientations (cases 2 and 3) ZINDO/S predicts similar trends.

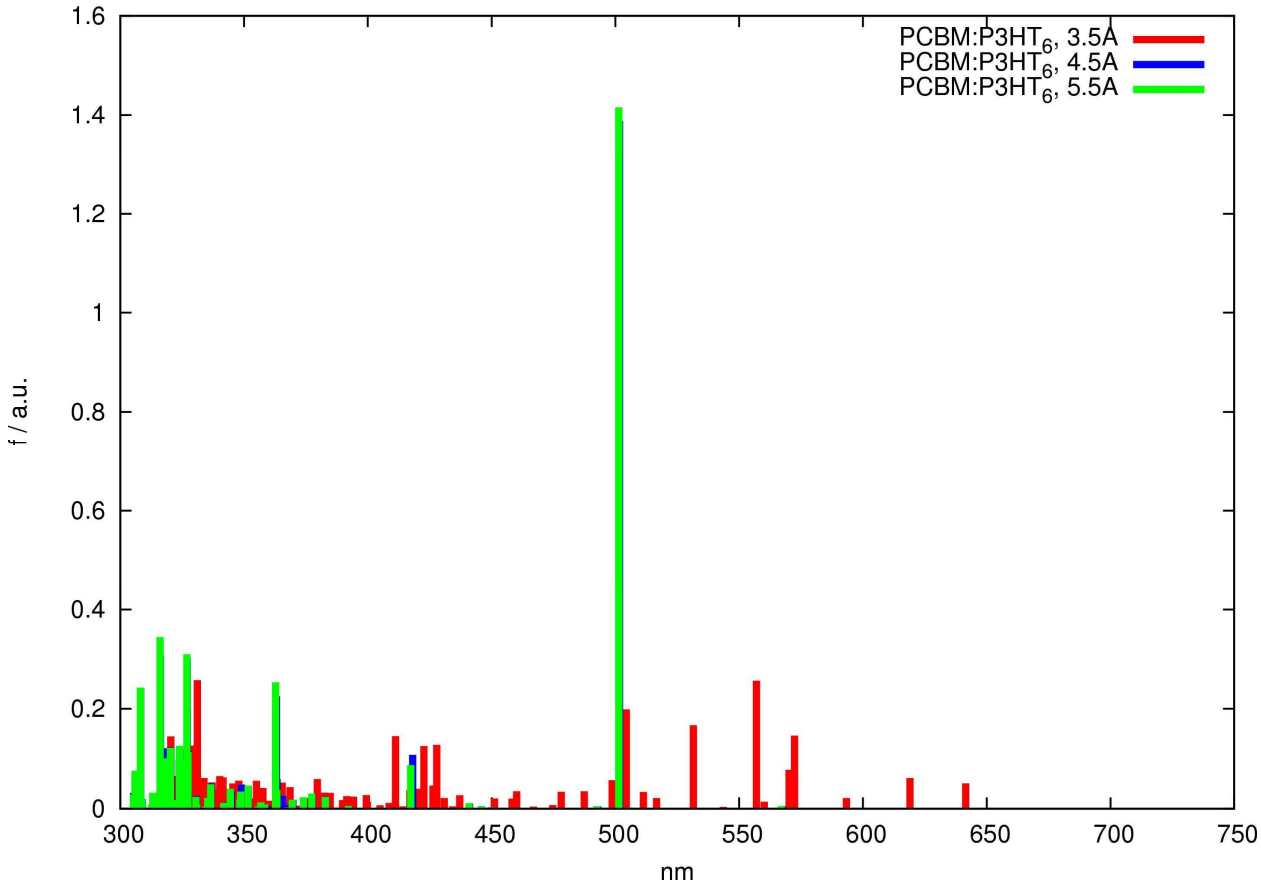

Figure S8: ZINDO/S vertical excitation energies and oscillator strength (f) calculated for P3HT/PCBM dimer case 1. For 3.5 Å intermolecular distance, it is clear the presence of new low lying excited states (as discussed in the paper) in the 600-650 nm range. For 4.5 and 5.5 Å the vertical transition energies are similar to those of the isolated molecules (see Figure S9).

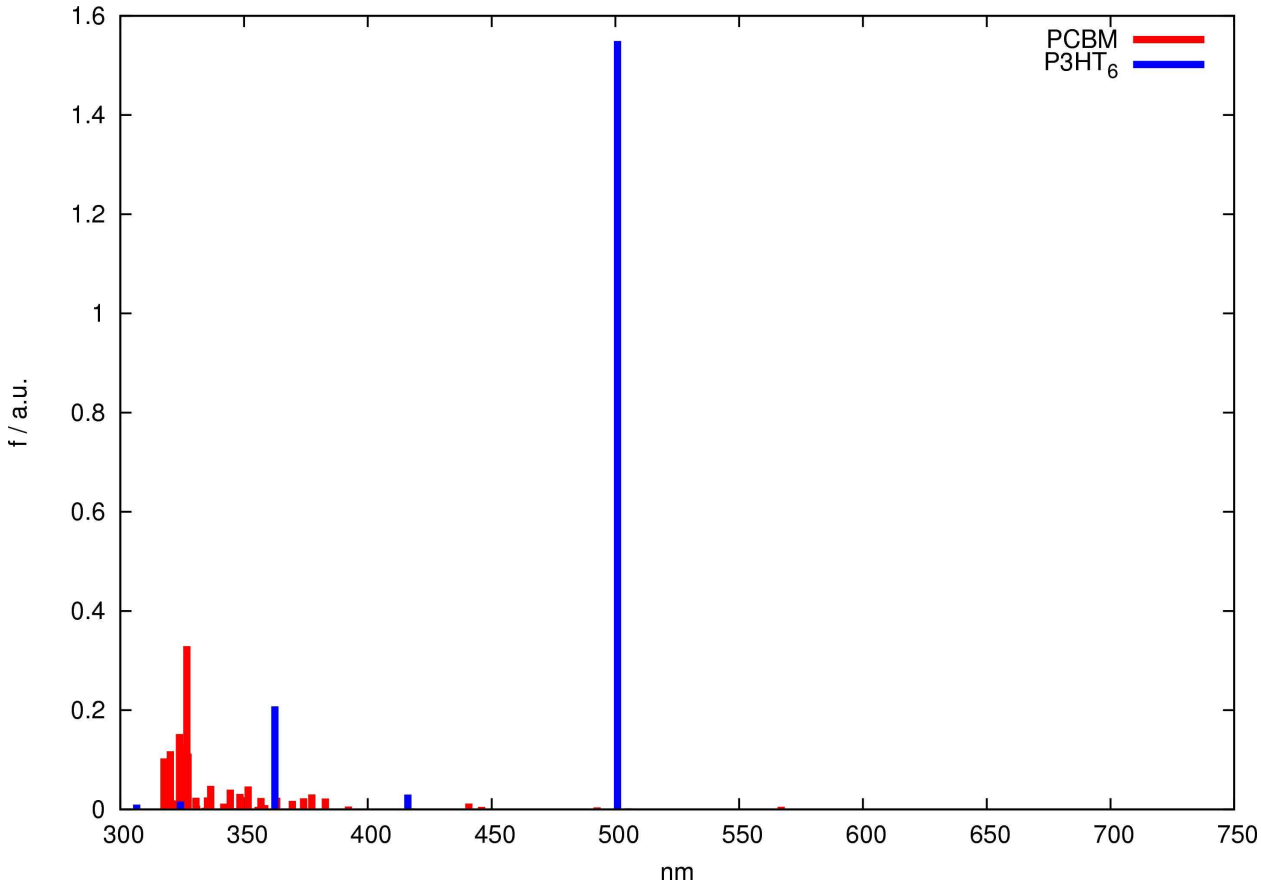

Figure S9: ZINDO/S vertical excitation energies and oscillator strength (f) calculated for optimized AM1 molecular structures of isolated P3HT and PCBM molecule.

Our results, even if they qualitatively support the experimental data, well describe the P3HT:PCBM BHJ and are in good agreement also with recent high level theoretical works [20,21]. All quantum chemical calculations have been carried out by using the Gaussian09 code [22].

SUPPORTING REFERENCES

1. Swinnen, A.; Haeldermans, I.; Vande, Ven M.; D'Haen, J.; Vanhoyland, G.; Aresu, S.; D'Olieslaeger, M.; Manca, J. Tuning the Dimensions of C_{60}-Based Needlelike Crystals in Blended Thin Films. *Adv. Funct. Mater* **2006**, *16*, 760-765.

2. Chirvase, D.; Parisi, J. C.; Hummelen, J. C.; Dyakonov, V. Influence of Nanomorphology on the Photovoltaic Action of Polymer–Fullerene Composites. *Nanotechnology* **2004**, *15,* 1317-1323.

3. Wang, T; Dunbar, A. D. F.; Staniec, P.A.; Pearson, A. J.; Hopkinson, P.E.; MacDonald, J.E.; Lilliu, S.; Pizzey, C.; Terrill, N. J.; Donald, A. M.; Ryan, A. J.; Jones, R. A. L.; Lidzey, D. G. The Development of Nanoscale Morphology in Polymer:Fullerene Photovoltaic Blends During Solvent Casting. *Soft Matter* **2010**, *6*, 4128-4134.

4. Korovyanko, O. J.; Österbacka, R.; Jiang, X. M.; Vardeny, Z. V.; Janssen, R. A. J. Photoexcitation Dynamics in Regioregular and Regiorandom Polythiophene Films. *Phys. Rev. B* **2001,** *64*, 235122-235127.

5. Marsh, R. A.; Hodgkiss, J. M.; Albert-Seifried, S.; Friend, R. Effect of Annealing on P3HT:PCBM Charge Transfer and Nanoscale Morphology Probed by Ultrafast Spectroscopy. *Nanoletter* **2010**, *10*, 923-930.

6. Guo, J.; Ohkita, H.; Benten, H.; Ito, S. Charge Generation and Recombination Dynamics in Poly(3-hexylthiophene)/Fullerene Blend Films with Different Regioregularities and Morphologies. *J. Am. Chem. Soc* **2010,** *132*, 6154-6164.

7. Cabanillas-Gonzalez, J.; Virgili, T.; Gambetta, A.; Lüer, L.; Lanzani, G. Subpicosecond Photoinduced Stark Spectroscopy in Fullerene-based Devices. *Phys. Rev. B* **2007**, *75*, 045207-045213.

8. Guo, J.; Ohkita, H.; Benten, H.; Ito, S. Near-IR Femtosecond Transient Absorption Spectroscopy of Ultrafast Polaron and Triplet Exciton Formation in Polythiophene Films with Different Regioregularities. *J. Am. Chem. Soc.* **2009**, *131*, 16869-16880.

9. Marchiori, C. F. N.; Koehler, M. Dipole Assisted Dissociation at Conjugated Polymer/Fullerene Photovoltaic Interfaces: A Molecular Study Using Density Functional Theory Calculations. *Synthetic Metals* **2010**, *160*, 643-650.

10. Dewar, M. J. S.; Zoebisch, E. G.; Healy, E. F. ; Stewart, J. J. P. Development and Use of Quantum Mechanical Molecular Models. 76.AM1: a New General Purpose Quantum Mechanical Molecular Model. *J. Am. Chem. Soc.* **1985**, *107* (13), 3902–3909.

11. Wang, Y.; Alcamì, M.; Martìn, F. Understanding the Supramolecular Self-Assembly of the Fullerene Derivative PCBM on Gold Surfaces. *Chem. Phys. Chem.* **2008***, 9,* 1030-1035.

12. Kanai, Y.; Grossman, J. C. Insights on Interfacial Charge Transfer Across P3HT/Fullerene Photovoltaic Heterojunction From Ab Initio Calculations. *Nano Lett.* **2007**, *7*, 1967-1972.

13. Yi, Y.; Coropceanu, V.; Brédas, J. L. Exciton-Dissociation and Charge Recombination Processes in Pentacene/C60 Solar Cells: Theoretical Insight into the Impact of the Interface Geometry. *J. Am. Chem. Soc.* **2009**, *131*, 15777-15783.

14. Huang, Y.; Westenhoff, S.; Avilov, I.; Sreearunothai, P.; Hodgkiss, J. M.; Deleener, C.; Friend, R. H.; Beljonne, D. Electronic Structures of Interracial States Formed at Polymeric Semiconductor Heterojunctions. *Nat Mater.* **2008**, *7*, 483-489.

15. Brédas, J. L.; Norton, J. E.; Cornil, J.; Coropceanu, V. Molecular Understanding of Organic Solar Cells: The Challenges. *Acc. Chem. Res.* **2009**, *42*, 1691-1699.

16. Cornil, J.; Beljonne, D.; Calbert, J. P.; Brédas, J. L. Interchain Interactions in Organic π-Conjugated Materials: Impact on Electronic Structure, Optical Response, and Charge Transport. *Adv. Mater.* **2001**, *13*, 1053-1067.

17. Brédas, J. L.; Beljonne, D.; Coropceanu, V.; Cornilal, J. Charge-Transfer and Energy-Transfer Processes in π-Conjugated Oligomers and Polymers: A Molecular Picture. *Chem. Rev.* **2004**, *104*, 4971-5003.

18. Zerner, M. C. Reviews of Computational Chemistry, Ed. K. B. Lipkowitz and D. B. Boyd, *2* (VCH Publishing, New York, **1991**) 313-66.

19. Marini, A.; Losa, A. M.; Biancardi, A.; Mennucci, B. What is Solvatochromism?, *J. Phys. Chem. B*, **2010**, *114*, 17128-17135.

20. Yi, Y.; Coropceanu, V.; Brédas, J. L. A Comparative Theoretical Study of Exciton-Dissociation and Charge-Recombination Processes in Oligothiophene/Fullerene and Oligothiophene/Perylenediimide Complexes for Organic Solar Cells, *J. Mater. Chem.* **2011**, *21*, 1479-1486

21. Liu, T.; Troisi, A. Absolute Rate of Charge Separation and Recombination in a Molecular Model of the P3HT/PCBM Interface, *J. Phys. Chem. C* **2011**, *115*, 2406-2415.

22. Frisch, M. J., et al. GAUSSIAN 09 (Revision A.02), Gaussian Inc., Wallingford CT, **2009**.